JOURNAL OF AIRCRAFT
Vol. 53, No. 6, November-December 2016

Performance and Energy Expenditure of Coflow Jet Airfoil with Variation of Mach Number

A. Lefebvre,* B. Dano,† W. B. Bartow,‡ M. D. Fronzo,§ and G. C. Zha¶
University of Miami, Coral Gables, Florida 33124

DOI: 10.2514/1.C033113

This paper conducts a numerical and experimental investigation of a coflow jet airfoil to quantify lift enhancement, drag reduction, and energy expenditure at a Mach number range from 0.03 to 0.4. The jet momentum coefficient is held constant at 0.08, and the angle of attack varies from 0 to 30 deg. The two-dimensional flow is simulated using a Reynolds–averaged Navier–Stokes solver with a fifth-order-weighted essentially non-oscillatory scheme for the inviscid flux and a fourth-order central differencing for the viscous terms. Turbulence is simulated with the one equation Spalart–Allmaras model. The predicted coflow jet pumping power has an excellent agreement with the experiment. At a constant Mach number, the power coefficient is decreased when the angle of attack is increased from 0 to 15 deg. When the Mach number is increased from 0.03 to 0.3, the suction effect behind the airfoil leading edge is further augmented due to the compressibility effect. This results in an increased maximum lift coefficient and reduced power coefficient at the higher Mach number because of the lower jet-injection pumping pressure required. At Mach 0.4, the lift coefficient is further improved. However as the angle of attack is increased, a λ shock wave interrupts the jet and triggers the boundary layer separation with increased drag and power coefficient. A corrected aerodynamic efficiency that includes the coflow-jet pumping power is introduced. Because of the high lift coefficient and low coflow-jet power required, the coflow-jet airfoil in this study achieves a comparable peak aerodynamic efficiency to the baseline airfoil, but the lift coefficient at peak efficiency is substantially increased by 120%. This study indicates that the coflow-jet airfoil is not only able to achieve very high maximum lift coefficient, but also able to improve cruise performance at low angle of attack when the flow is benign.

Nomenclature

C_D	=	drag coefficient
C_L	=	lift coefficient
C_p	=	pressure coefficient
c_p	=	constant pressure specific heat
H_t	=	total enthalpy, joule
$(L/D)_c$	=	corrected aerodynamic efficiency for coflow-jet airfoil $L/(D + P/V_\infty)$
M	=	Mach number
$\dot{m}$	=	mass flow rate of the coflow jet, kg/s
P	=	pumping power consumption, Watt
P_c	=	power coefficient
P_t	=	total pressure, Pascal
R_e	=	Reynolds number
S	=	planform area of the wing, m^2
T_t	=	total temperature, k^o
V_∞	=	velocity, m/s
γ	=	air specific-heats ratio
ρ_∞	=	density, kg/m^3

Subscripts

∞	=	free stream
j	=	jet

I. Introduction

A SUCCESSFUL active flow control (AFC) should provide a substantial improvement in aerodynamic performance, which may include enhancement of lift and aerodynamic efficiency, drag reduction, and stall margin increase. The energy expenditure should remain low to make the AFC beneficial. A desirable AFC method will enhance airfoil performance by energizing the flow with minimal or no structural moving parts.

The circulation control (CC) airfoil is one of the major airfoil AFCs that the research community has studied for several decades [1–4]. CC airfoil relies on the Coanda effect, which creates a favorable pressure gradient on a curved surface to prevent flow separation. Such a favorable pressure gradient exists at the airfoil leading edge (LE) due to the LE suction and in the vicinity of a blunt trailing edge (TE) due to the low base pressure. Hence, a blunt TE is usually required to render the CC effective. However, a thick TE increases drag at cruise condition. To overcome the dependence on a blunt TE for CC airfoil, a movable flap at the airfoil TE is suggested by Englar [5]. But moving parts impose a weight penalty. At large angles of attack (AoA), the flow cannot overcome the large adverse pressure gradient. As a result, a favorable pressure gradient near the TE cannot be achieved and, hence, the Coanda effect is difficult to realize. If only TE blowing is used, a CC airfoil stalls at a smaller AoA than a noncontrolled airfoil. To maintain sufficient stall margin, LE blowing also needs to be added [6]. A considerable penalty of the blowing on the overall aircraft system efficiency is the dumped blowing jet mass flow, which may be induced from the propulsion system bleed or other pumping systems. Furthermore, for a CC airfoil, the drag measured in a wind tunnel is not the actual drag that occurs in flight, because the penalty to draw the mass flow from the freestream as the supply for the jet injection is not included in the drag measurement. The actual drag, also called equivalent drag, needs to include this penalty [4,7]. To mitigate the penalty, a pulsed jet CC airfoil is shown to effectively reduce the jet mass flow rate [4].

Presented as Paper 2013-0490 at the 51st AIAA Aerospace Sciences Meeting, Grapevine, TX, 7–10 January 2013; received 22 September 2014; revision received 8 February 2016; accepted for publication 27 February 2016; published online 6 June 2016.

*Ph.D. Candidate, Dept. of Mechanical and Aerospace Engineering; lefebvrealexis@gmail.com.
†Adjunct Faculty, Dept. of Mechanical and Aerospace Engineering; bertrand_dano@hotmail.com.
‡Master Student, Dept. of Mechanical and Aerospace Engineering; wbartow@miami.edu.
§Visiting Master Student, Dept. of Mechanical and Aerospace Engineering; difronzomichele@gmail.com.
¶Professor; gzha@miami.edu. Associate Fellow AIAA.

Other promising flow-control methods, including the zero-net mass flux (ZNMF) synthetic jets [8,9] and dielectric-barrier discharge plasma actuators [10,11], are being developed to suppress flow separation. These approaches avoid dumping the jet mass flow. However, at present, both synthetic jets and plasma actuators generally lack sufficient actuator authority for high-speed flows. Overall, most of the current airfoil AFCs are aimed at increasing maximum lift coefficient by suppressing flow separation or using the Coanda effect. Few AFC techniques are able to improve the airfoil performance at cruise condition when the flow is benign at low AoA.

Recently, a promising ZNMF coflow jet (CFJ) flow-control airfoil developed by Zha et al. [7,12–19] achieved a radical lift augmentation, drag reduction, and stall margin increase at a low energy expenditure [7,17]. In addition to augmenting the maximum lift coefficient with increased circulation and high-stall AoA, the CFJ airfoil also is shown to have a very appealing feature: it could significantly increase the airfoil lift coefficient and aerodynamic efficiency at cruise condition with low AoA from the subsonic to transonic regime [20–22]. This superior advantage at cruise condition so far is demonstrated mostly by numerical simulation [20–22]. The experimental proof of CFJ airfoil cruise performance enhancement is the next step.

A. The Coflow Jet Airfoil

In the CFJ airfoil concept [7,12–18], an injection slot near the LE and a suction slot near the TE are created on the airfoil suction surface as shown in Fig. 1. A small amount of mass flow is withdrawn into the airfoil near the TE, pressurized and energized by a pumping system inside the airfoil, and then injected near the LE in the direction tangent to the mainflow. The whole process does not add any mass flow to the system and hence is a ZNMF flow control.

The CFJ airfoil has a unique low-energy-expenditure mechanism. It has the injection slot near the LE suction peak of the airfoil where the lowest mainflow pressure is located. The low mainflow pressure makes the jet easy to be injected into the flow. At the same time, the suction slot is located near the TE, where the mainflow pressure is the highest. The high pressure of the mainflow makes the flow easy to be withdrawn into the suction slot. The CFJ airfoil total pumping power is hence lower than the flow-control methods that have injection only near the TE, such as a CC airfoil. The injection and suction of a CFJ airfoil are synergized, and they both enhance boundary-layer momentum and airfoil circulation.

The fundamental mechanism of the CFJ airfoil is that the turbulent mixing between the jet and mainflow energize the wall boundary layer. The large vortex structures and adverse pressure gradient are beneficial to enhance mixing. The mixing allows the flow to overcome a large adverse pressure gradient and to remain attached at a very high AoA. Hence, the stall margin is significantly increased. At the same time, the energized boundary layer drastically increases the circulation, augments lift, and reduces the total drag or generates thrust (net negative drag). Unlike a jet in crossflow (JICF), which enhances mixing between the jet and mainflow but retards the mainflow due to the crossflow blockage created by the jet, the CFJ mixing only enhances the streamwise flow momentum, because the jet is tangential to the mainflow. The momentum retardation due to JICF will result in a significant entropy and drag increase.

A CFJ airfoil reduces drag while increasing the lift. The drag reduction could be so large that thrust (i.e., negative drag) can be generated. The thrust generation or drag reduction by a CFJ airfoil can be explained by two mechanisms [7,12–14]: First, due to the very high circulation, the LE suction is so strong that the low pressure at the LE results in a thrust. The slightly increased local surface friction due to higher jet velocity is offset by this LE supersuction, or pressure drag reduction, which is the same mechanism that bird wings use to generate thrust during downstroke flapping at high AoA. Second, the energized mainflow fills the wake and reduces the velocity deficit. From control volume analysis, it is known that a shallower wake velocity deficit means a smaller drag. When the wake velocity deficit is reversed, the airfoil will generate thrust, which occurs for the CFJ airfoil as demonstrated in both experiment and numerical simulation [7,12–17]. CFJ airfoils appear to be the only flow-control method that generates both significant lift and thrust at the same time.

Figure 2 shows a massive flow separation of the baseline NACA 6415 airfoil at AoA of 25 deg in our wind tunnel testing [16]. Figure 3 is the particle image velocimetry (PIV) measured velocity field with CFJ at the same AoA, which demonstrates that the flow is attached with a higher speed within the wake than in the freestream, creating a reversed wake deficit. In this case, thrust is generated. The flow is attached at a momentum coefficient C_μ of 0.06 for this case. Figure 4 shows the coherent vortex structure in the vicinity of the injection slot from our experimental flow visualization with $C_\mu = 0.02$.

Figure 5 compares the measured lift coefficient of several discrete CFJ (DCFJ) airfoils with the baseline airfoil at a constant jet mass flow rate [16,17]. The DCFJ airfoils in Fig. 5 have different slot blockages to generate discrete injection holes, and hence different jet velocity, while keeping the same mass flow rate. For example, the open slot (black solid circles) has zero blockage. The obstruction factor (OF; i.e., blockage), indicated after "DCFJ" in the figure legend, is the percentage of the slot area blocked. An OF of 3/4 means that 75% of the injection slot area is blocked, and it results in many small discrete holes for the CFJ injection. Figure 5 shows that the open-slot CFJ airfoil increases the maximum lift coefficient by about 50%, whereas the discrete CFJ airfoil with OF of 2/3 increases the lift by about 100%. When the mass flow is increased, the measured maximum lift coefficient is further augmented, as shown in Fig. 6.

Figure 6 shows all the airfoils generate thrust (negative drag) in the wind tunnel testing, with the maximum amount produced by a CFJ airfoil using discrete jets with OF of 3/4. The minimum drag is reduced by 4000% to an enormous thrust coefficient of about 0.8. By comparing with the open-slot CFJ airfoil, the discrete CFJ airfoil needs half of the mass flow rate to achieve the same lift augment and drag reduction [17]. However, the power consumed by the DCFJ is significantly higher than for the open-slot CFJ airfoil, because the

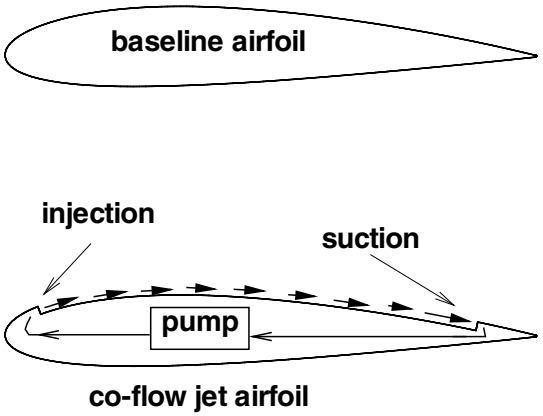

Fig. 1 Baseline airfoil and CFJ airfoil.

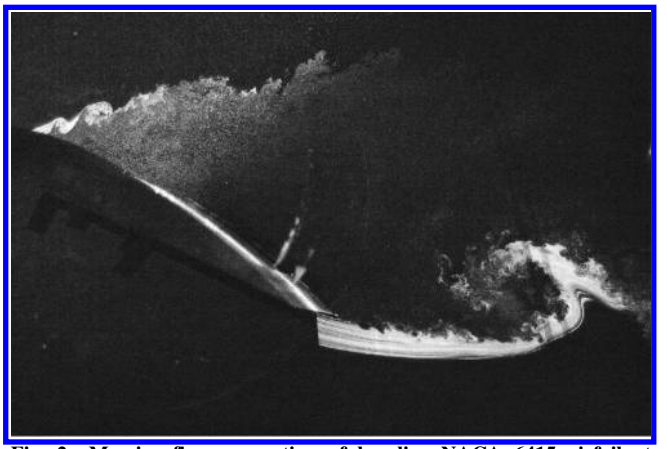

Fig. 2 Massive flow separation of baseline NACA 6415 airfoil at AoA = 25 deg.

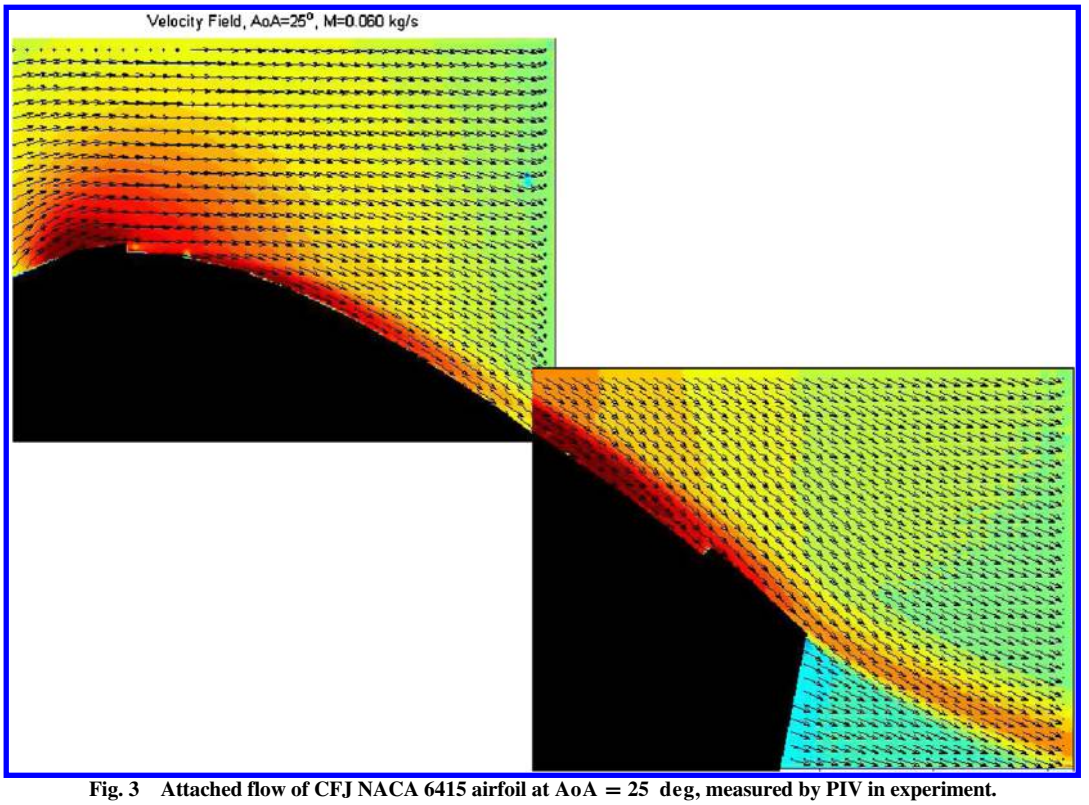

Fig. 3 Attached flow of CFJ NACA 6415 airfoil at AoA = 25 deg, measured by PIV in experiment.

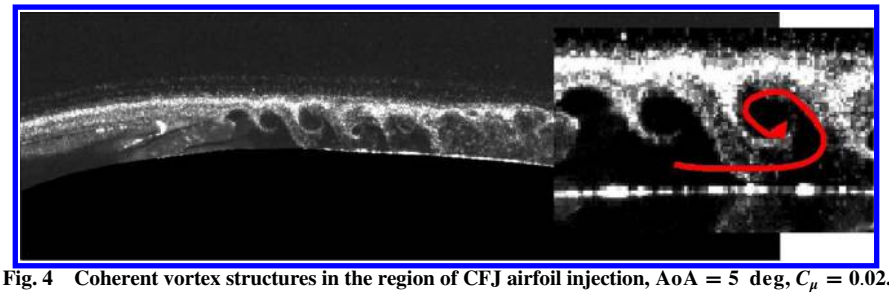

Fig. 4 Coherent vortex structures in the region of CFJ airfoil injection, AoA = 5 deg, $C_\mu = 0.02$.

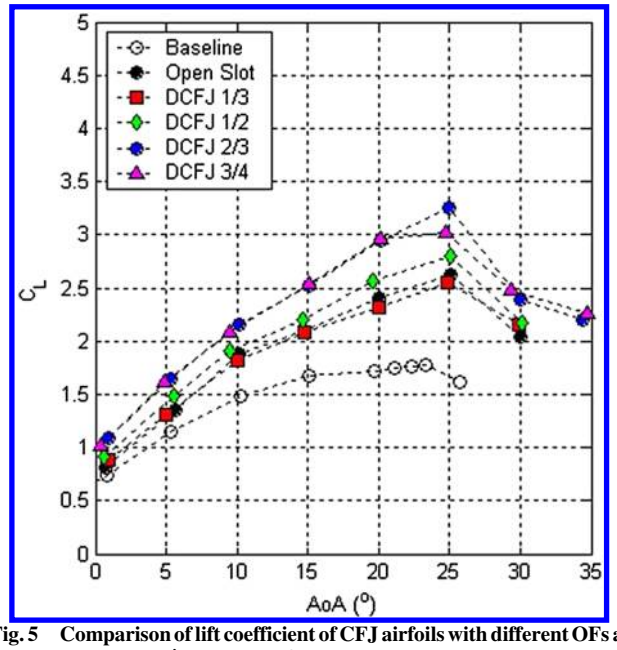

Fig. 5 Comparison of lift coefficient of CFJ airfoils with different OFs at constant mass flow $\dot{m} = 0.03$ kg/s.

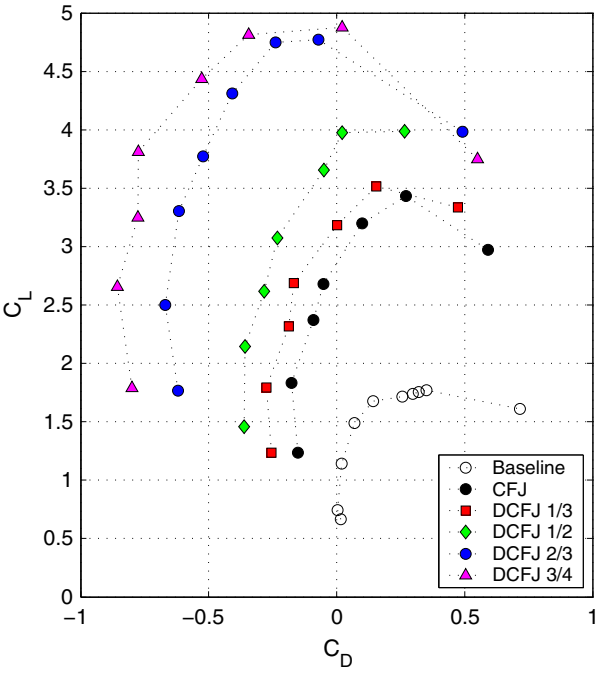

Fig. 6 Comparison of the drag polars of DCFJ airfoils with different OFs at constant mass flow $\dot{m} = 0.06$ kg/s.

smaller holes create more blockage loss for the jets. Nonetheless, the extraordinary high lift and high thrust generated by the DCFJ deserve the extra energy cost [17]. In nature, the only system that generates both lift and thrust at the same time is flapping bird wings. In the man-made fixed wing systems, CFJ airfoils appear to be the only system that can achieve such effect.

Dano et al. [17] experimentally investigated the energy expenditure at Mach number of 0.03. Their study indicates that the CFJ airfoil gains drastic performance enhancement at high AoA for a low energy expenditure. Additional numerical studies performed by Lefebvre et al. [23,24] confirm the trends. However, no study has been conducted to investigate CFJ airfoil performance enhancement and energy expenditure with Mach number effect.

B. Objectives

The purpose of this paper is to study CFJ airfoil energy expenditure and performance enhancement with the variation of Mach number from 0.03 to 0.4. When the incoming Mach number is greater than 0.2, the compressibility effect plays an important role. Such knowledge is important to expand the CFJ airfoil application to a wider Mach number range and to different phases in a flight mission. An important potential application of CFJ airfoils is for pitching airfoils in a rotorcraft blade [25] to remove dynamic stall, which experiences a wide variation of incoming-flow Mach number during one rotor revolution. In particular, there is no study for CFJ airfoils with incoming Mach number up to 0.4. Such a Mach number range will usually generate a transonic flowfield with shock wave–boundary layer interaction, which may reduce the effectiveness of a flow control. Studying the CFJ airfoil aerodynamic performance at this Mach number range is important to determine if it is suitable for a system where a transonic flow may be induced.

II. CFJ Parameters

This section introduces the definitions of several parameters that are important to describe CFJ airfoil performance.

A. Lift and Drag Calculation

The momentum and pressure at the injection and suction slots produce a reactionary force, which is automatically measured by the force balance in wind tunnel testing. However, for CFD simulation, the full reactionary force needs to be included. Using control volume analysis, the reactionary force can be calculated using the flow parameters at the injection and suction-slot opening surfaces. Zha et al. [7] give the following formulations to calculate the lift and drag due to the jet reactionary force for a CFD simulation. By considering the effects of injection and suction jets on the CFJ airfoil, the expressions for these reactionary forces are given as

$$F_{x_{\mathrm{CFJ}}} = (\dot{m}_j V_{j1} + p_{j1}A_{j1}) \times \cos(\theta_1 - \alpha) - (\dot{m}_j V_{j2} + p_{j2}A_{j2}) \times \cos(\theta_2 + \alpha) \tag{1}$$

$$F_{y_{\mathrm{CFJ}}} = (\dot{m}_{j1} V_{j1} + p_{j1}A_{j1}) \times \sin(\theta_1 - \alpha) + (\dot{m}_{j2} V_{j2} + p_{j2}A_{j2}) \times \sin(\theta_2 + \alpha) \tag{2}$$

in which the subscripts 1 and 2 stand for the injection and suction respectively, and θ_1 and θ_2 are the angles between the injection and suction-slot surfaces and a line normal to the airfoil chord. α is the AoA.

The total lift and drag on the airfoil can then be expressed as

$$D = R'_x - F_{x_{\mathrm{CFJ}}} \tag{3}$$

$$L = R'_y - F_{y_{\mathrm{CFJ}}} \tag{4}$$

in which R'_x and R'_y are the surface integral of pressure and shear stress in x (drag) and y (lift) direction, excluding the internal ducts of injection and suction. For the computational fluid dynamics (CFD) simulation, the total lift and drag are calculated using Eqs. (3) and (4).

B. Jet Momentum Coefficient

The jet momentum coefficient C_μ is a parameter used to quantify the jet intensity. It is defined as

$$C_\mu = \frac{\dot{m} V_j}{\frac{1}{2}\rho_\infty V_\infty^2 S} \tag{5}$$

in which $\dot{m}$ is the injection mass flow, V_j the injection velocity, ρ_∞ and V_∞ denote the freestream density and velocity, and S is the planform area.

C. Power Coefficient

The CFJ can be implemented by mounting a pumping system inside the wing that withdraws air from the suction slot and blows it into the injection slot. The power consumption can be determined by the jet mass flow and total enthalpy change as the following:

$$P = \dot{m}(H_{t1} - H_{t2}) \tag{6}$$

in which H_{t1} and H_{t2} are the total enthalpy in the injection cavity and suction cavity respectively, P is the power required by the pump, and $\dot{m}$ is the jet mass flow rate. Introducing the pump efficiency η and total pressure ratio of the pump $\Gamma = (P_{t1}/P_{t2})$, the power consumption can be expressed as

$$P = \frac{\dot{m} C_p T_{t2}}{\eta}(\Gamma^{\frac{\gamma-1}{\gamma}} - 1) \tag{7}$$

The power consumption can be expressed as a power coefficient:

$$P_c = \frac{P}{\frac{1}{2}\rho_\infty V_\infty^3 S} \tag{8}$$

D. Corrected Aerodynamic Efficiency

The conventional airfoil aerodynamic efficiency is defined as L/D. However, because CFJ AFC consumes energy, the CFJ airfoil corrected aerodynamic efficiency is modified to take into account the energy consumption of the pump. The formulation of the corrected aerodynamic efficiency for CFJ airfoils is

$$\left(\frac{L}{D}\right)_c = \frac{L}{D + \frac{P}{V_\infty}} \tag{9}$$

in which V_∞ is the freestream velocity, P is the CFJ pumping power, and L and D are the lift and drag generated by the CFJ airfoil. This formulation converts the power consumed by the CFJ into the drag of the airfoil. If the pumping power is set to 0, this formulation returns to the aerodynamic efficiency of a conventional airfoil.

III. CFD Simulation Setup

A. CFD Code

The FASIP (Flow-Acoustics-Structure Interaction Package) CFD code is used to conduct the numerical simulation. The two-dimensional Reynolds-averaged Navier–Stokes (RANS) equations with the one-equation Spalart-Allmaras [26] turbulence model is used. A fifth-order weighted essentially nonoscillatory (WENO) scheme for the inviscid flux [27–32] and a fourth-order central differencing for the viscous terms [27,31] are employed to discretize the Navier–Stokes equations. The low-diffusion energy-convection upstream spliting pressure scheme used as the approximate Riemann solver, suggested by Zha et al. [28], is used with the WENO scheme to evaluate the inviscid fluxes. An implicit time-marching method using Gauss–Seidel line relaxation is used to achieve a fast convergence rate [33]. Parallel computing is implemented to save wall clock

Table 1 Block dimension for CFJ 6415 airfoil

Block	ξ-Direction	η-Direction	Cell number
1–9	51	101	5000
10	101	31	3000
11	151	31	4500
12	101	31	3000
Total mesh size	— —	— —	55500

simulation time [34]. The RANS solver is validated with the CFJ airfoil simulation [15,35–37].

B. Boundary Conditions

The third-order accuracy no-slip condition is enforced on the solid surface with the wall treatment suggested in [38] to achieve the flux conservation on the wall. Total pressure, total temperature, and flow angles are specified as the inlet boundary conditions for the upstream portion of the far-field boundary and inside the injection cavity. Constant static pressure is used for the downstream portion of the far-field boundary and inside the suction cavity.

To achieve zero net mass flux with the CFJ flow control, the mass flow exiting the injection slot must be equal to the mass flow entering the suction slot. Additionally, the jet strength must be controlled in order to reach the prescribed C_μ. The prescribed C_μ is achieved by adjusting the injection cavity total pressure. Total temperature is assumed constant during this process. The injection and suction mass flow are matched by adjusting the suction cavity static pressure. The process is iterated throughout the simulation until the specified momentum coefficient is reached and the injection and suction mass flow match within the tolerance of 1%.

C. Mesh

The two-dimensional mesh is constructed using the O-mesh topology in order to achieve high-quality mesh around the airfoil. A total of 451 points are placed around the airfoil, 301 points on the suction surface, 151 points on the pressure surface, and 101 points normal to the airfoil, with an additional 31 points across the jet. The total mesh size is 55,500 cells and is partitioned into 12 blocks for parallel computation. The far-field boundary is located 30 chord away from the airfoil. To resolve the turbulent boundary layer, the first grid point is placed at $y^+ \approx 1$. The block definition is found in Table 1, and the mesh topology is shown in Fig. 7.

A mesh refinement was performed at $M = 0.3$ by increasing the mesh size by 50% in every direction. The results are in excellent agreement with the baseline mesh.

IV. Wind Tunnel Experiments [16–18]

All airflow and aerodynamic variables are acquired at the University of Miami $24'' \times 24'' \times 48''$ wind tunnel facilities. The experimental measurements are performed at $M = 0.03$ and $Re = 2 \times 10^5$. LE trip is used to render the boundary layer fully turbulent

The baseline airfoil tested in the wind tunnel experiments is a NACA 6415 airfoil with the chord length of $12''$ and span of $24''$. The CFJ 6415 airfoil is constructed from the NACA 6415 with the injection and suction located at 7.5 and 88.5% of the chord,

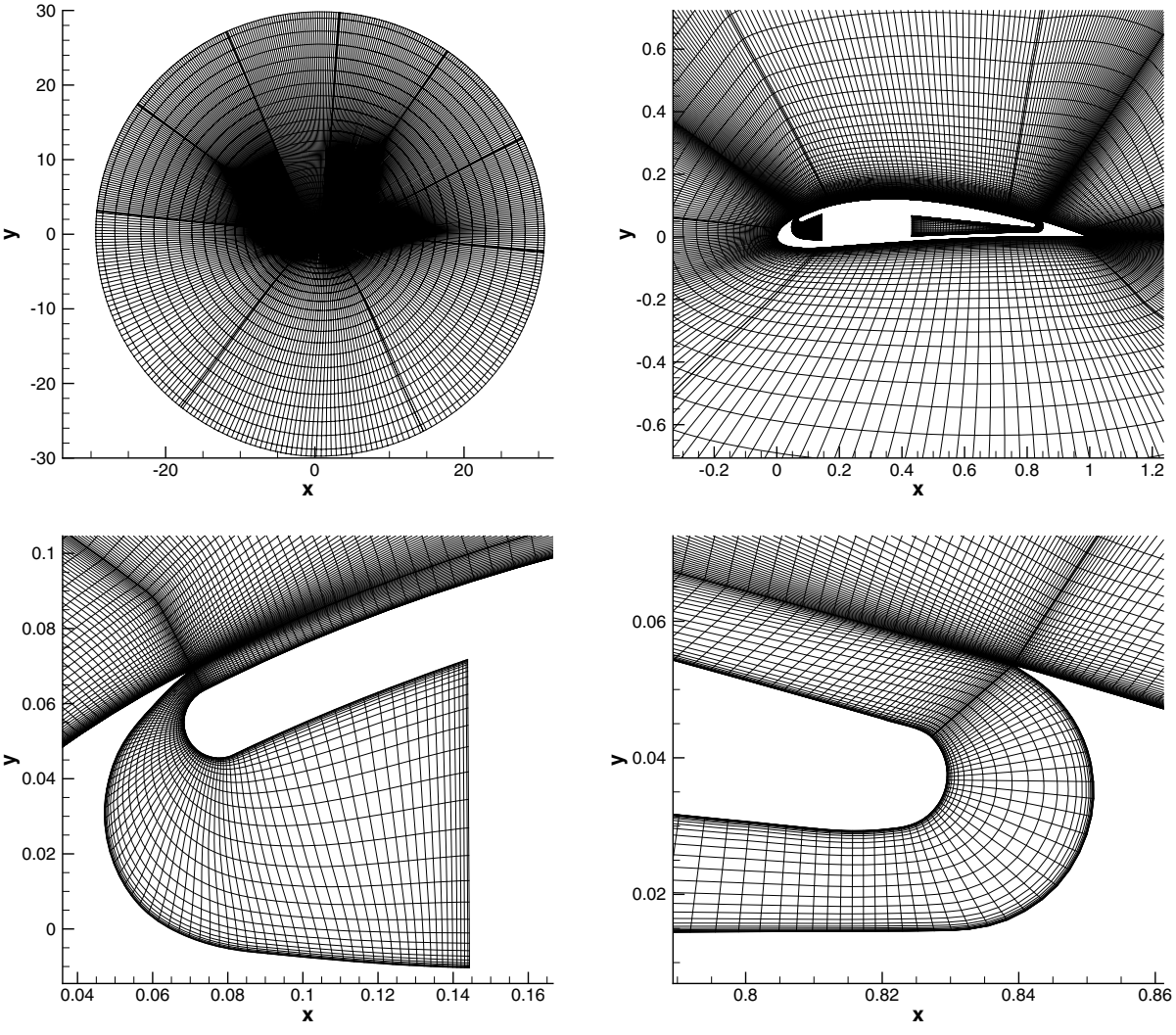

Fig. 7 CFJ 6415 two-dimensional O-mesh topology with detailed view of the injection and suction cavities.

Table 2 Reynolds number variation with freestream velocity and Mach number

Mach	V_∞ (m/s)	Reynolds number ($\times 10^5$)
0.03	10.297	2.078
0.3	102.968	20.779
0.4	137.290	27.705

respectively. The injection and suction-slot heights are 0.65% (2.0 mm) and 1.30% (4.0 mm) of the chord. In the experiment, the CFJ is generated by a separated high-pressure source for the injection and a low-pressure vacuum sink for the suction. Pressurized air is injected into a spanwise cavity near the LE and exits through a rectangular slot across the span. A Duocel high-density aluminum foam is placed between the inlet and the injection slot to equilibrate the pressure and ensure a uniform exit velocity. Similarly, a spanwise cavity along the span placed near the TE is used to withdraw the air for the suction.

The injection and suction flow conditions are independently controlled in the experiment. A compressor supplies the high pressure injection flow line and the flow rate is controlled using a Koso™ Hammel Dahl computer-controlled valve. A vacuum pump generates the necessary low pressure for suction and is controlled with a manual needle valve. Both mass flow rates in the injection and suction lines are measured using Oripac™ orifice mass flow meters equipped with high-precision pressure transducers. Total pressure and temperature probes are placed inside the injection and suction cavities. The aerodynamics variables are measured using an AMTI™ six-component transducer. All the data (e.g., wind tunnel speed, aerodynamic forces, blowing and suction mass flow rates) are acquired at a rate of 50 samples/s using a state-of-the-art Labview™ data acquisition system. The measurement uncertainty of the forces, total pressure, total temperature, and mass flow rate is within 1%.

V. Results

The CFJ 6415 airfoil, which is experimentally studied by Dano et al. in [16–18] at $M = 0.03$, is first simulated to validate the CFD solver. The Mach number is then increased to 0.3 and 0.4. The jet momentum coefficient is held constant at $C_\mu = 0.08$ for all the Mach numbers. The AoA varies from 0 to 30 deg, in increments of 5 deg. The Reynolds numbers based on freestream velocity and chord length are listed in Table 2.

A. CFD Validation at $M = 0.03$

Figure 8 shows the computed lift and drag coefficient compared with the experiment for the baseline airfoil and the CFJ airfoil at $M = 0.03$. For the lift, a good agreement is obtained up to AoA of 20 deg when the flow is mostly attached. The CFD underpredicts the stall AoA by about 5 deg for both the baseline and CFJ airfoil. The computed drag coefficient is significantly underpredicted when the AoA is greater than 10 deg. This appears to be due to the RANS turbulence model, which cannot accurately predict the drag at high AoA when the flow is close to stalling or stalled [37,39].

However, the predicted power coefficient shown in Fig. 9 agrees excellently with the experiment. In Fig. 9, the left vertical axis represents the dimensionless power coefficient, whereas the right vertical axis is the required pumping power in watt. The reason why the predicted power consumption agrees well with the experiment may be that the total pressure and total temperature are integrated parameters using mass average and are predicted more accurately as lump parameters. It is observed that the power coefficient decreases with the increase of AoA up to 15 deg and then rises at higher AoA. The reason is that, when the AoA is increased and the flow still remains attached, the airfoil LE suction effect becomes stronger with lower static pressure in the region of the injection jet, and hence less

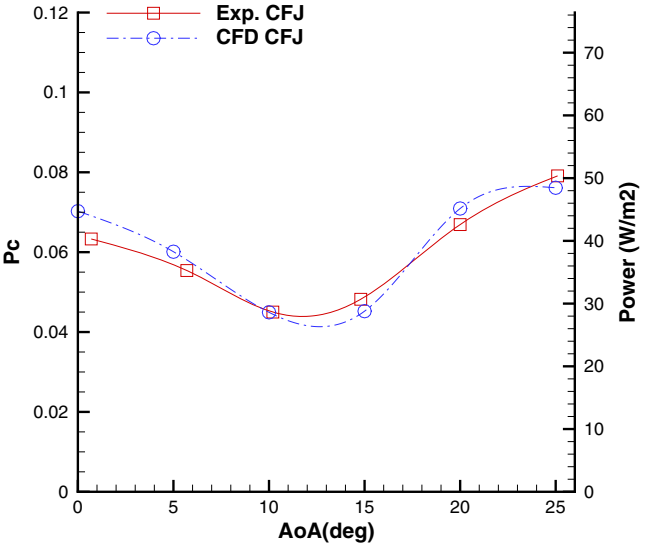

Fig. 9 Computed power coefficient compared with experiment at $M = 0.03$ and $C_\mu = 0.08$.

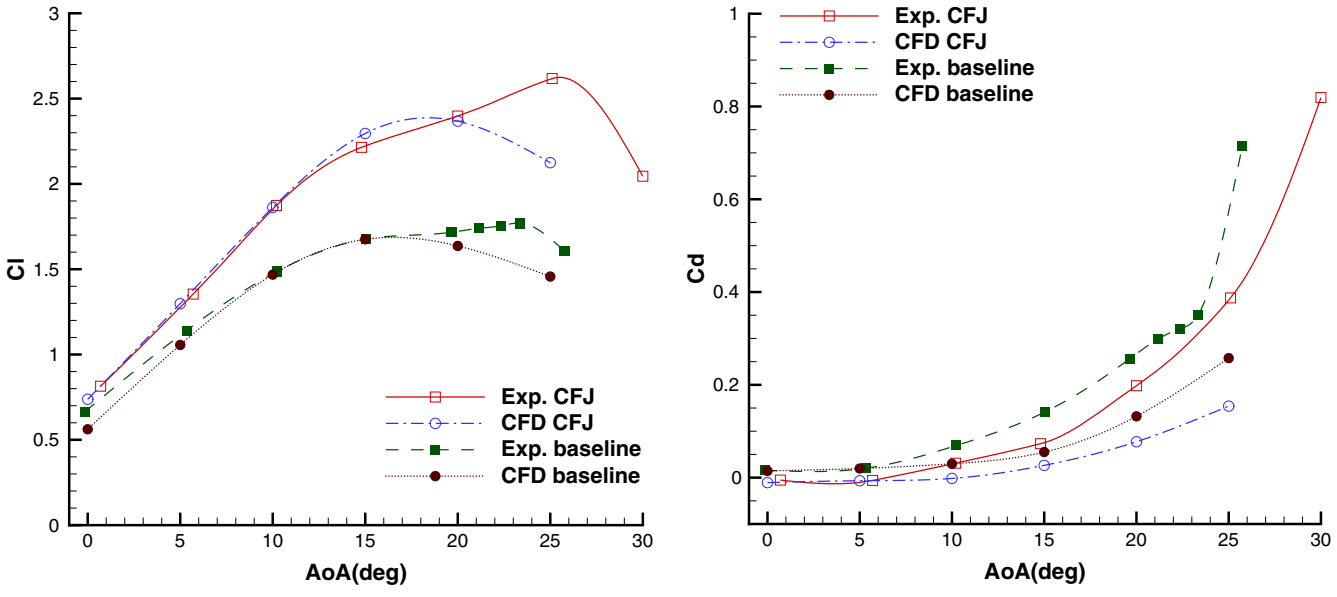

Fig. 8 Lift and drag coefficient comparison between experiment and CFD at $M = 0.03$ and $C_\mu = 0.08$.

power is needed to generate the jet with the same momentum coefficient. However, when the AoA is beyond the separation value, the boundary layer separation creates large energy loss and the suction power is significantly increased. Overall, the excellent agreement of the predicted power coefficient with the experiment lays the foundation for further study at higher Mach number.

B. Performance at High Mach Number: 0.3 and 0.4

Figure 10 shows the computed lift, drag, and power coefficient at Mach number from 0.03 to 0.4. The baseline airfoil lift and drag have little dependency on the freestream Mach number and hence are plotted at $M = 0.3$ only. With the Mach number increased from 0.03 to 0.4, the maximum lift coefficient of the CFJ airfoil is increased from 2.2 to 2.8 with $C_\mu = 0.08$. This is due to the compressibility effect at higher Mach number, which generates a stronger suction effect at the LE. However, at $M = 0.4$, the airfoil stalls earlier due to the appearance of a strong shock wave on the suction surface as to be shown later. The drag coefficient is also significantly increased at Mach 0.4 when the AoA is greater than 15 deg due to the shock wave–boundary layer interaction and wave drag. The power coefficient decreases when the Mach number is increased from 0.03 to 0.3. This is due to the compressibility effect that lowers the static pressure of the mainflow at the injection region, which in turn reduces the pumping energy required to create the jet. At $M = 0.4$, the power coefficient at AoA $= 0$ deg is about the same as at Mach 0.3 and is significantly lower than at Mach 0.03. However, with the AoA increased up to 15 deg, the power coefficient at Mach 0.4 remains fairly flat instead of decreasing as at Mach 0.3. The reason is that the flow reaches supersonic at high AoA, and the energy loss is increased as well, in particular when shock waves appear as shown later. When the AoA is greater than 15 deg, the strong shock wave–boundary layer interaction generates very large entropy increase and makes the power required increase significantly. Figure 10 also shows the 1.5×1.5 refined mesh results for C_L, C_D, and P_c at Mach 0.3. They are virtually identical to the baseline mesh results and indicate that the present CFD simulations are converged based on the mesh size.

The results above are plotted as drag polars in Fig. 11. The left polar is the pure aerodynamic lift versus drag plot. The right polar, however, is the corrected aerodynamic efficiency $(L/D)_c$, accounting for the pumping power by adding the power coefficient to the drag coefficient as explained in Eq. (9). This plot shows that the CFJ airfoil performs more efficiently than the baseline airfoil for $C_L \geq 1.5$, at which the baseline airfoil is about to be stalled.

Figure 12 shows the pressure coefficient on the baseline and CFJ 6415 airfoil surfaces at various AoA for a freestream Mach number of 0.03 and 0.3. The spikes on the CFJ airfoil pressure distribution are due to the injection and suction slots. The CFJ greatly increases the circulation on the suction surface due to increased flow velocity, which augments the lift. The lift augment is greater at higher AoA. The CFJ airfoil has a significantly higher suction peak near the LE than does the baseline airfoil, which contributes to the lift increase and the pressure drag decrease. For the CFJ airfoil, the higher freestream Mach number reduces the suction side pressure more than the baseline airfoil because the CFJ enhances the compressibility effect.

Figures 13–15 show the Mach number contours with streamlines for the CFJ 6415 airfoil at various AoAs for a freestream Mach

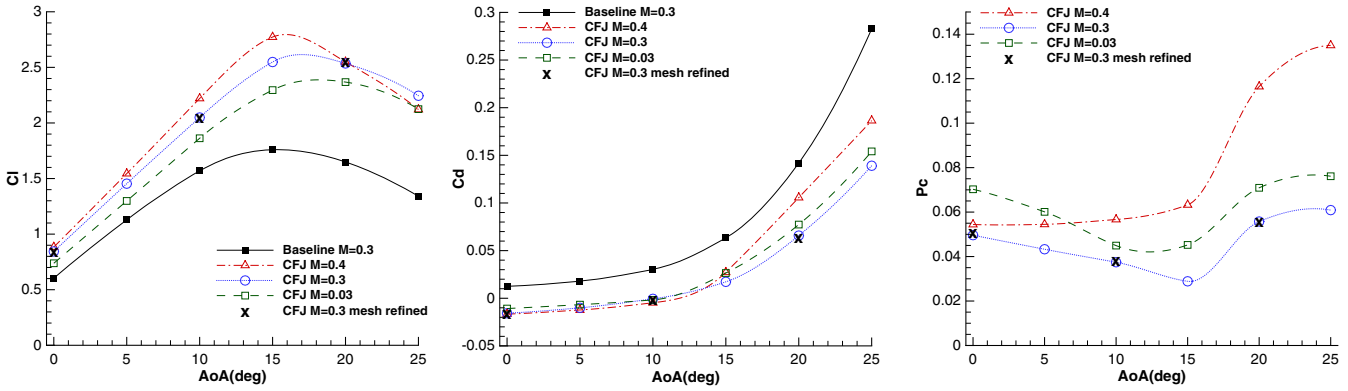

Fig. 10 Lift, drag, and power comparison from $M = 0.03$ to 0.4 and $C_\mu = 0.08$.

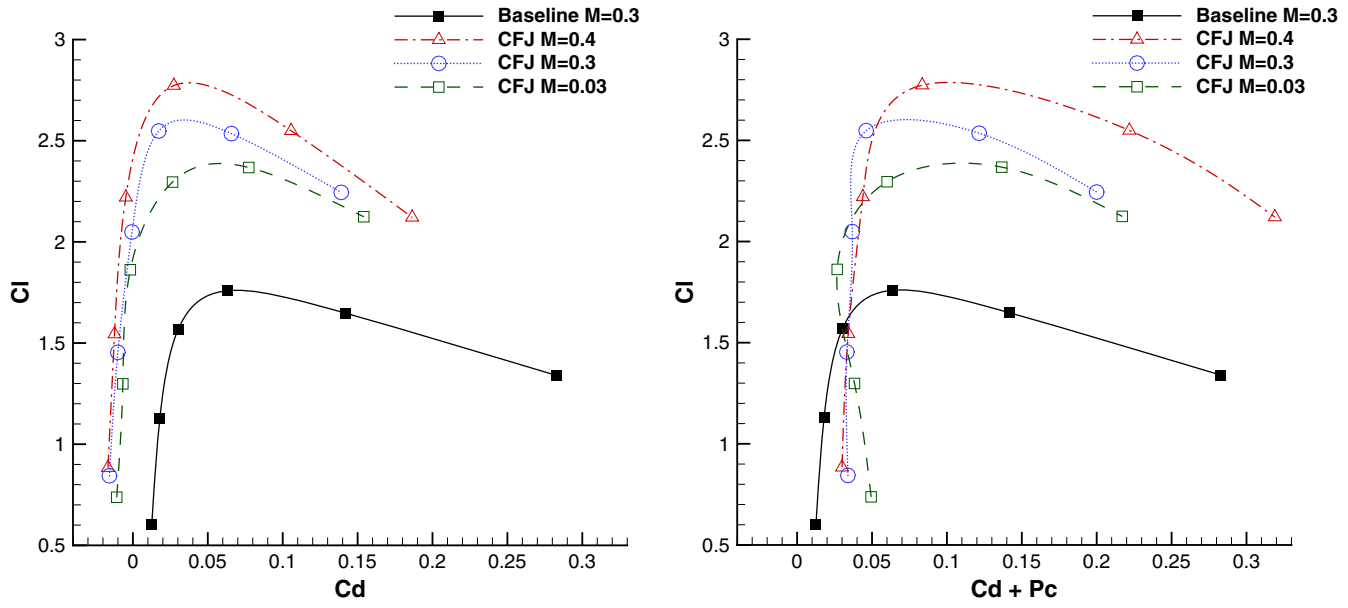

Fig. 11 Drag polar (left) and drag polar corrected to account for the pumping power (right) at various Mach numbers and $C_\mu = 0.08$.

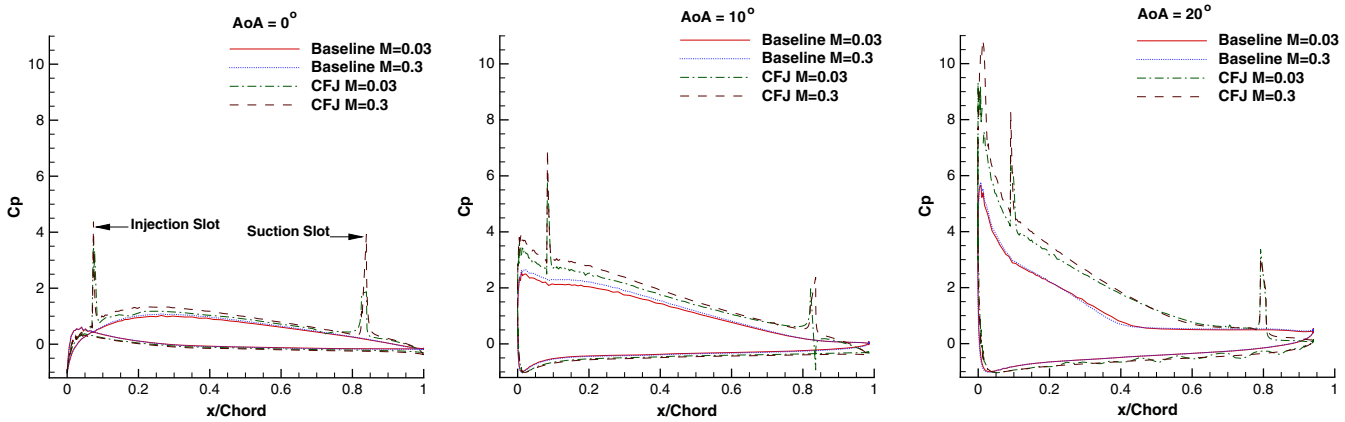

Fig. 12 Pressure coefficient comparison between the CFJ and the baseline airfoil from $M = 0.03$ to 0.3 and $C_\mu = 0.08$.

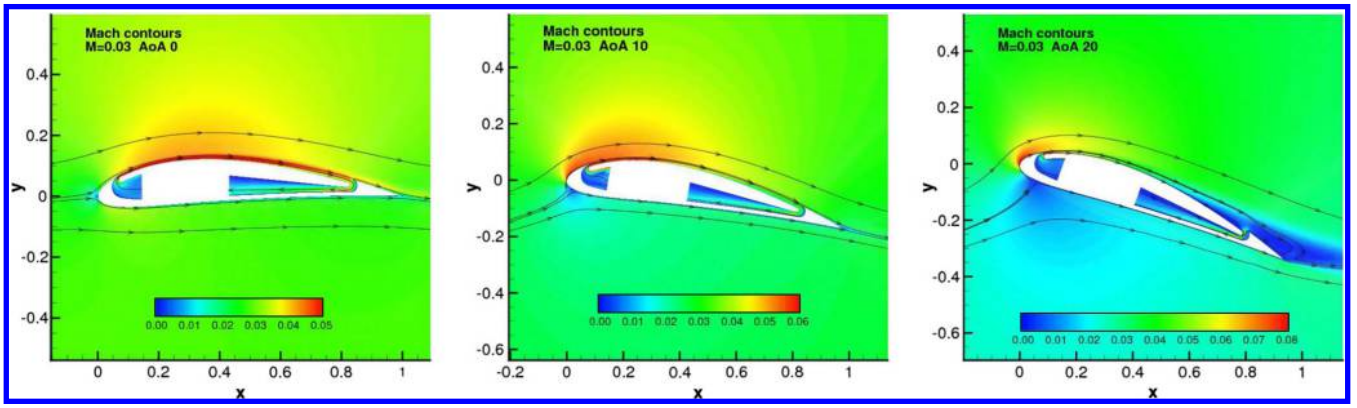

Fig. 13 CFJ 6415 airfoil Mach contours at $M = 0.03$ and $C_\mu = 0.08$ for AoAs of 0 deg (left), 10 deg (middle), and 20 deg (right).

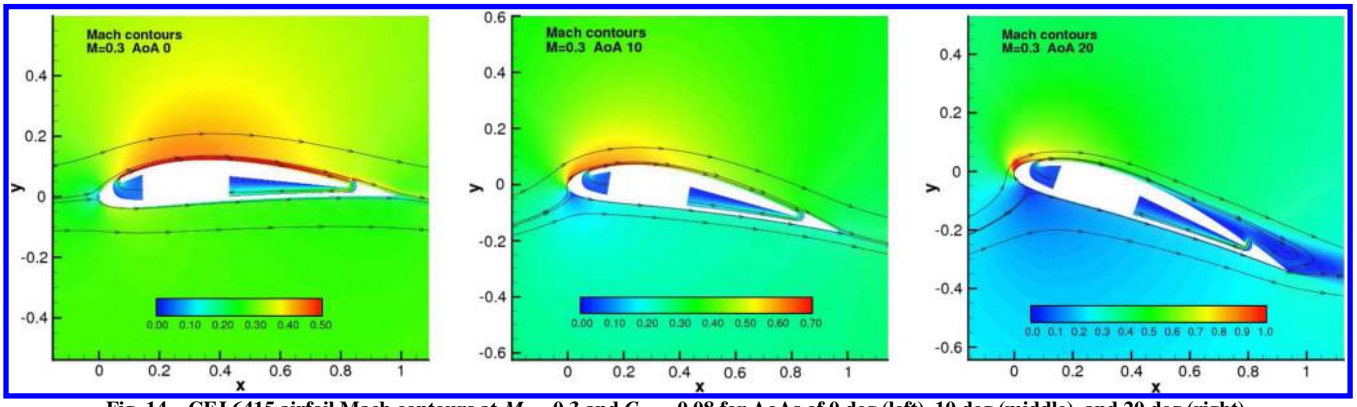

Fig. 14 CFJ 6415 airfoil Mach contours at $M = 0.3$ and $C_\mu = 0.08$ for AoAs of 0 deg (left), 10 deg (middle), and 20 deg (right).

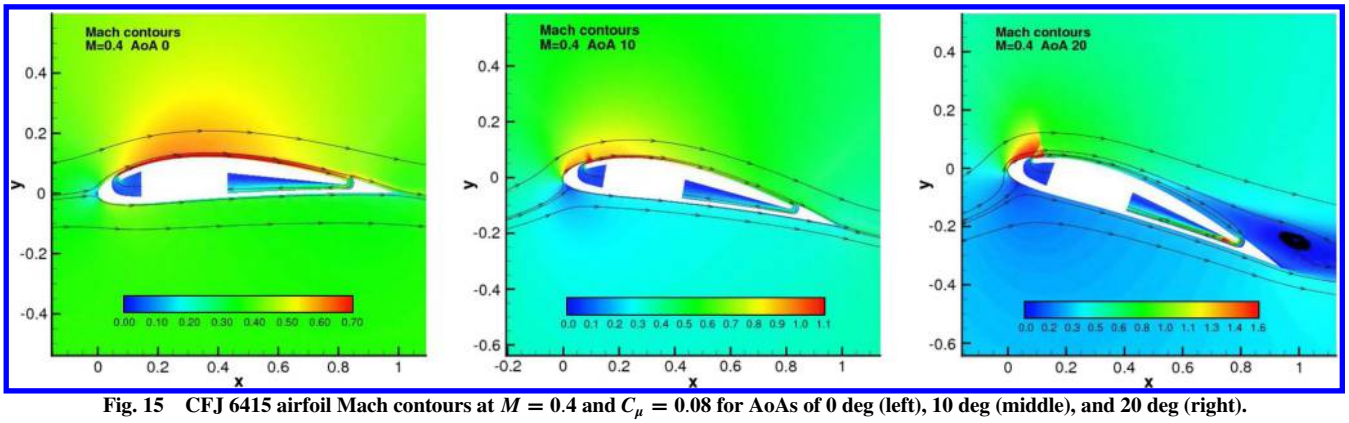

Fig. 15 CFJ 6415 airfoil Mach contours at $M = 0.4$ and $C_\mu = 0.08$ for AoAs of 0 deg (left), 10 deg (middle), and 20 deg (right).

number of 0.03, 0.3, and 0.4 respectively. The CFJ enhances the suction surface acceleration very effectively. At AoA = 20 deg, there is a mild separation near the TE for Mach 0.03 and 0.3. The separation can be easily removed by increasing C_μ slightly, such as to 0.12 [23,24]. In general, the flowfield structures of Mach 0.03 and 0.3 are very much the same. However, when the Mach number is increased to 0.4, the flowfield structure is changed to the appearance of a shock wave at the injection jet region. The shock wave–boundary layer interaction triggers a flow separation.

Figures 16–18 show the Mach number contours at the injection jet region for a freestream Mach number of 0.03, 0.3, and 0.4 respectively at AoA = 0, 10, and 20 deg. At $M = 0.03$, the flowfield with CFJ is subsonic as expected. When the Mach number is increased to 0.3, the jet exit velocity is transonic. At AoA = 20 deg, a supersonic region appears in the LE region with the maximum Mach number about 1.4. A freestream Mach number of 0.3 is still very favorable for lift increase and drag reduction at low power expenditure because the relatively weak shocks are still in the near isentropic region. When the Mach number reaches 0.4, the flowfield structure is very different, characterized by supersonic flow and shock waves in the injection region as shown in Fig. 18. At AoA = 0 deg, the injection jet already reaches Mach 1.5. At AoA = 10 deg, the injection jet speed is further increased due to the decreased mainflow static pressure at the injection region, and a weak shock forms downstream of the injection slot. However, the jet remains uninterrupted. At AoA = 20 deg, the injection jet Mach number reaches 2.2. A strong λ shock appears in the injection region. The rear leg of the λ shock has greater strength, interrupts the jet, and causes significant flow separation, thus increasing the drag and power coefficient and reducing the stall AoA as shown in Fig. 10.

Figure 19 is the comparison of the corrected aerodynamic efficiency $(L/D)_c$ defined in Eq. (9) for the baseline and CFJ airfoil at different Mach numbers. The Mach 0.3 case has higher peak aerodynamic efficiency and lift coefficient than does the Mach 0.03 case. This is benefited from the flow compressibility that enhances the LE suction effect. The peak efficiency AoA of the CFJ airfoil is at

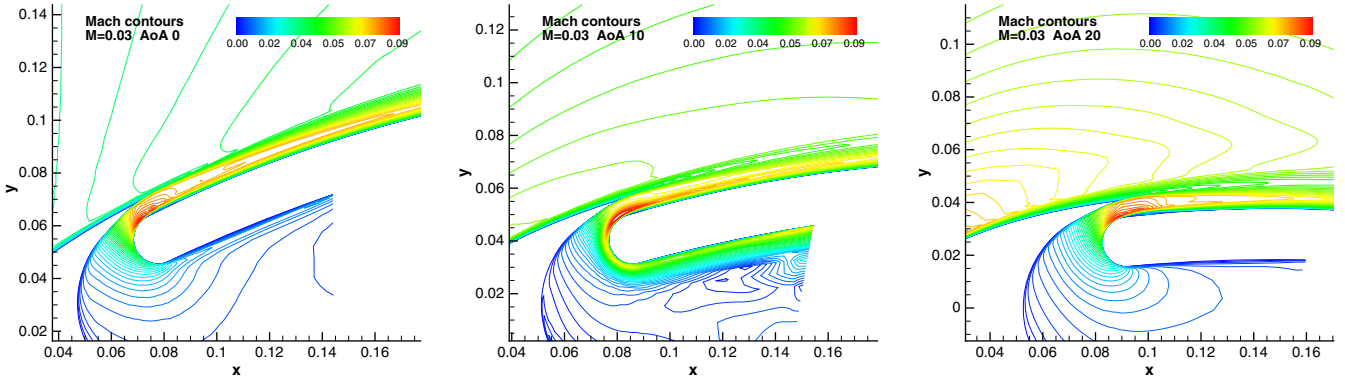

Fig. 16 Jet-injection region Mach number line contours at $M = 0.03$ and $C_\mu = 0.08$ for AoAs of 0 deg (left), 10 deg (middle), and 20 deg (right).

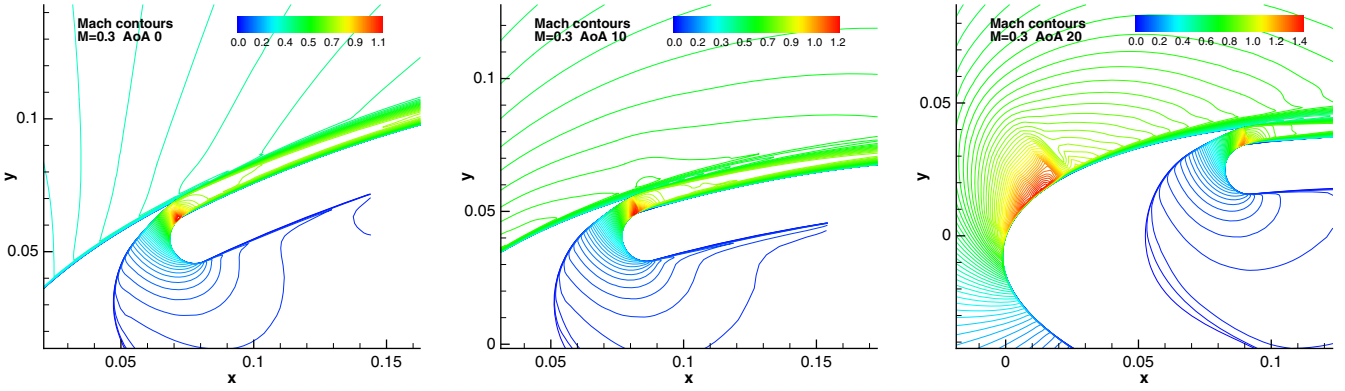

Fig. 17 Jet-injection region Mach number line contours at $M = 0.3$ and $C_\mu = 0.08$ for AoAs of 0 deg (left), 10 deg (middle), and 20 deg (right).

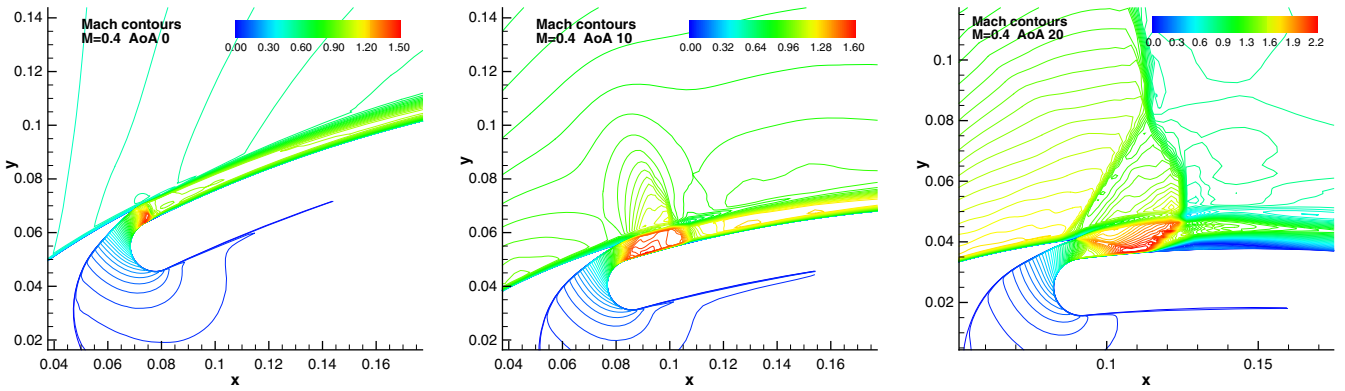

Fig. 18 Jet-injection region Mach number line contours at $M = 0.4$ and $C_\mu = 0.08$ for AoAs of 0 deg (left), 10 deg (middle), and 20 deg (right).

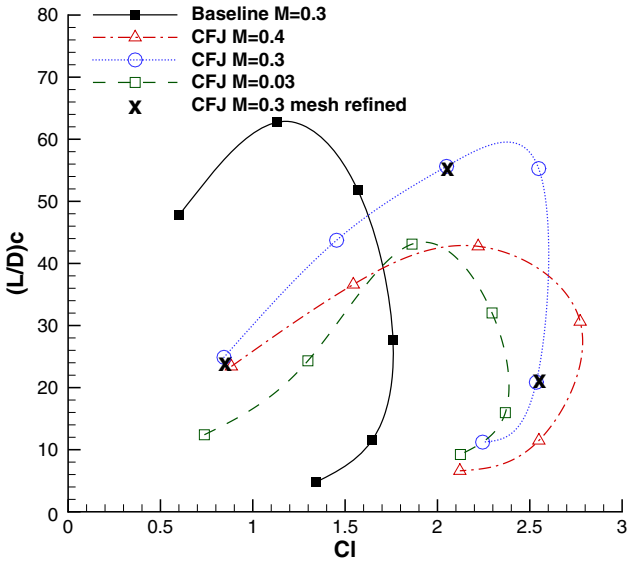

Fig. 19 Comparison of corrected aerodynamic efficiency between baseline and CFJ airfoil at different Mach numbers at $C_\mu = 0.08$.

about 13 deg, substantially higher than that of the baseline airfoil at 5 deg. This phenomenon is because the lowest CFJ pumping power is at that AoA at which the lift enhancement is high and the drag is very low, because the flow is not near separation. This also indicates that the cruise AoA of a CFJ airfoil would be higher than a conventional airfoil. At Mach 0.4, the peak efficiency drops due to the appearance of strong shock waves. This is partially because that the NACA6415 airfoil is a subsonic airfoil and is not suitable to handle transonic flow. For the Mach number of 0.3 that gives a mostly subsonic flowfield with no strong shock wave–boundary layer interaction, the peak efficiency of the CFJ airfoil is only dropped by about 4% compared with the baseline airfoil, but the lift coefficient is increased by about 120%. With a systematic optimization, it is believed that this CFJ airfoil's peak efficiency, measured by $(L/D)_c$, can surpass that of the baseline airfoil. This is a very appealing advantage. With a comparable aerodynamic efficiency as the baseline airfoil, the substantially increased lift coefficient means that a CFJ airplane can have much higher wing loading and smaller wing size for the same payload or, for the same size, the CFJ airplane can carry much more payload or more fuel for a longer range. A smaller wing size means weight reduction, which will contribute to the overall system efficiency. Using this advantage, Lefebvre and Zha [20] achieve a conceptual design of an electric airplane using a CFJ wing that has wing loading nearly three times higher than that of conventional design, which at least doubles the range by carrying much more battery. This very encouraging result is also extended to transonic airfoil. Liu and Zha [22] apply the CFJ flow control to a transonic supercritical RAE2822 airfoil with rigorous numerical simulation. It increases the peak aerodynamic effciency $(L/D)_c$ by 14.5% and at the same time augments the lift coefficient by 18.7%. If all these are proved to be true experimentally, the CFJ airfoil flow-control technology will bring a revolution for future aircraft design. Experimental proof of the CFJ airfoil performance enhancement at cruise condition is the next step.

One factor that is not considered in this study is the perceived pumping system weight, which is difficult to define at this stage because different designs may employ different pumping systems. However, the weight penalty in general is not considered as significant because the overall pumping pressure ratio is very low, typically on the order of 1.02 to 1.04 but always lower than 1.1. That means the pump blades will not sustain a large load; hence, light material can be used, for example, the plastic blades of computer cooling fans. Because the lift coefficient increase is enormous, it will significantly reduce the wing structure size and weight. The weight penalty of pumping system is expected to be minimal and may be negligible.

VI. Conclusions

The performance enhancement and energy expenditure of the CFJ-6415 airfoil with the Mach number varying from 0.03 to 0.4 is investigated numerically and experimentally. The momentum coefficient of 0.08 is kept constant during the study. The two-dimensional RANS solver with high-order schemes and Spalart–Allmaras model is used to simulate the baseline and CFJ-6415 airfoils. The CFD underpredicts the stall AoA, but the predicted lift coefficient agrees very well with the measurement until the numerical simulated flow is stalled. The predicated drag coefficient also agrees well with experiment at low AoA but is significantly underestimated at high AoA. Even though the lift and drag coefficient have large discrepancy at high AoA when the flow is near stall, the predicted CFJ pumping power coefficient agrees very well with the measurement through the whole AoA range. This appears to be because the power coefficient is determined by the mass averaged injection and suction total pressure ratio as lump parameters, which can be more accurately predicted by the CFD simulation than the skin friction.

The maximum lift coefficient is increased with the increasing Mach number due to the compressibility effect. However, at $M = 0.4$, the airfoil stalls with slightly lower AoA due to the appearance of a λ shock wave that interrupts the jet and triggers the boundary layer separation. The drag coefficient varies less with the Mach number but is substantially increased at Mach 0.4 when the AoA is high due to shock wave–boundary layer interaction and wave drag. At a constant Mach number, the power coefficient is decreased when the AoA is increased from 0 to 15 deg. This is because the increased AoA enhances the LE suction effect, which allows lower pumping power to achieve the same momentum coefficient. When the Mach number is increased from 0.03 to 0.3, the suction effect behind the airfoil LE is further augmented due to a compressibility effect. This results in an increased maximum lift coefficient and reduced power coefficient at the higher Mach number because of the lower jet-injection pumping pressure required. The drag coefficient remains fairly stable with the Mach number variation.

Because of the appearance of shock waves at $M = 0.4$ when the AoA is high, the power coefficient is significantly increased. Overall, the study indicates that the CFJ airfoil is very effective to enhance lift, reduce drag, and increase stall margin with Mach number up to 0.4. Energy expenditure is low for Mach number up to 0.3 but is significantly increased at Mach 0.4. The most efficient AoA is in the range 10–15 deg, at which the CFJ lift is high and the power coefficient is the lowest. This also indicates that the cruise AoA of a CFJ airfoil will be typically higher than a conventional airfoil. As long as the flow of the CFJ airfoil is in the subsonic regime with no shock wave, the higher the Mach number, the higher the enhancement of peak aerodynamic efficiency and lift coefficient, which benefit from the flow compressibility. Because of the significantly increased lift coefficient and very low CFJ power required, the CFJ airfoil has a very appealing advantage: it has about the same peak aerodynamic efficiency as that of the baseline airfoil, but the lift coefficient at peak efficiency is substantially increased by 120%. It means that the CFJ airfoil is not only able to substantially increase maximum lift coefficient, but also able to improve cruise performance at low AoA.

Acknowledgments

All the simulations were conducted at the Center for Computational Sciences (CCS) at the University of Miami. The teaching assistantship for the first author from the University of Miami is gratefully acknowledged.

References

[1] Englar, R., and Williams, R. M., "Test Techniques for High Lift, Two-Dimensional Airfoils with Boundary Layer and Circulation Control for Application to Rotary Wing Aircraft," *Canadian Aeronautics and Space Journal*, Vol. 19, No. 3, 1973, pp. 93–108.

[2] Englar, R. J., "Circulation Control for High Lift and Drag Generation on STOL Aircraft," *Journal of Aircraft*, Vol. 12, No. 5, 1975, pp. 457–463. doi:10.2514/3.59824

[3] Englar, R. J., Trobaugh, L. A., and Hemmersly, R., "STOL Potential of the Circulation Control Wing for High-Performance Aircraft," *Journal of Aircraft*, Vol. 14, No. 3, 1978, pp. 175–181.

[4] Jones, G. S., "Pneumatic Flap Performance for a 2D Circulation Control Airfoil, Steady & Pulsed," *Applications of Circulation Control Technologies*, edited by Joslin, R. D., and Jones, G. S., Vol. 214, Progress in Astronautics and Aeronautics, AIAA, Reston, VA, 2006, pp. 191–244, Chap. 7.

[5] Englar, R. J., "Circulation Control Pneumatic Aerodynamics: Blown Force and Moment Augmentation and Modifications; Past, Present and Future," AIAA Paper 2000-2541, 2000.

[6] Liu, Y., Sankar, L. N., Englar, R. J., Ahuja, K. K., and Gaeta, R., "Computational Evaluation of the Steady and Pulsed Jet Effects on the Performance of a Circulation Control Wing Section," *42nd AIAA Aerospace Sciences Meeting and Exhibit*, AIAA Paper 2004-0056, 2004.

[7] Zha, G.-C., Gao, W., and Paxton, C., "Jet Effects on Co-Flow Jet Airfoil Performance," *AIAA Journal*, Vol. 45, No. 6, 2007, pp. 1222–1231.

[8] Glezer, A., and Amitay, M., "Synthetic Jets," *Annual Review of Fluid Mechanics*, Vol. 24, No. 34, 2002, pp. 503–529.

[9] Holman, R., Utturkar, Y., Mittal, R., and Cattafesta, L., "Formation Criterion for Synthetic Jets," *AIAA Journal*, Vol. 43, No. 10, 2005, pp. 2110–2116.
doi:10.2514/1.12033

[10] Corke, T. C., and Post, M. L., "Overview of Plasma Flow Control: Concepts, Optimization, and Applications," AIAA Paper 2005-0563, 2005.

[11] Enloe, C., McLaughlin, T. E., Font, G. I., and Baughn, J. W., "Frequency Effects on the Efficiency of Aerodynamic Plasma Actuator," AIAA Paper 2006-0166, 2006.

[12] Zha, G.-C., and Paxton, D. C., "A Novel Flow Control Method for Airfoil Performance Enhancement Using Co-Flow Jet," *Applications of Circulation Control Technologies*, edited by Joslin, R. D., and Jones, G. S., Vol. 214, Progress in Astronautics and Aeronautics, AIAA, Reston, VA, 2006, pp. 293–314, Chap. 10.

[13] Zha, G.-C., Paxton, C., Conley, A., Wells, A., and Carroll, B., "Effect of Injection Slot Size on High Performance Co-Flow Jet Airfoil," *Journal of Aircraft*, Vol. 43, No. 4, 2006, pp. 987–995.

[14] Zha, G.-C., Carroll, B., Paxton, C., Conley, A., and Wells, A., "High Performance Airfoil with Co-Flow Jet Flow Control," *AIAA Journal*, Vol. 45, No. 8, 2007, pp. 2087–2090.

[15] Wang, B.-Y., Haddoukessouni, B., Levy, J., and Zha, G.-C., "Numerical Investigations of Injection Slot Size Effect on the Performance of Co-Flow Jet Airfoil," *Journal of Aircraft*, Vol. 45, No. 6, 2008, pp. 2084–2091.

[16] Dano, B. P. E., Kirk, D., and Zha, G.-C., "Experimental Investigation of Jet Mixing Mechanism of Co-Flow Jet Airfoil," *Fifth AIAA Flow Control Conference*, AIAA Paper 2010-4421, 2010.

[17] Dano, B. P. E., Zha, G.-C., and Castillo, M., "Experimental Study of Co-Flow Jet Airfoil Performance Enhancement Using Micro Discreet Jets," *49th AIAA Aerospace Sciences Meeting*, AIAA Paper 2011-0941, 2011.

[18] Dano, B., Lefebvre, A., and Zha, G.-C., "Flow Mixing Mechanism of a Discrete Co-Flow Jet Airfoil," *41st AIAA Fluid Dynamics Conference and Exhibit*, AIAA Paper 2011-3097, 2011.

[19] Lefebvre, A., Dano, B., Di Franzo, M., Bartow, W., and Zha, G.-C., "Performance of Co-Flow Jet Flow Airfoil with Variation of Mach Number," *51st AIAA Aerospace Science Meeting*, AIAA Paper 2013-0490, 2013.

[20] Lefebvre, A., and Zha, G.-C., "Design of High Wing Loading Compact Electric Airplane Utilizing Co-Flow Jet Flow Control," *AIAA SciTech2015: 53nd Aerospace Sciences Meeting*, AIAA Paper 2015-0772, 2015.

[21] Lefebvre, A., and Zha, G.-C., "Trade Study of 3D Co-Flow Jet Wing for Cruise Performance," *AIAA SCITECH2016, AIAA Aerospace Science Meeting*, AIAA Paper 2016-0570, Jan. 2016.

[22] Liu, Z.-X., and Zha, G.-C., "Transonic Airfoil Performance Enhancement Using Co-Flow Jet Active Flow Control," *8th AIAA Flow Control Conference*, AIAA, Reston, VA, June 2016.

[23] Lefebvre, A., and Zha, G.-C., "Co-Flow Jet Airfoil Trade Study Part I: Energy Consumption and Aerodynamic Performance," *Proceedings of the AIAA Flow Control Conference*, AIAA, Reston, VA, June 2014.

[24] Lefebvre, A., and Zha, G.-C., "Co-Flow Jet Airfoil Trade Study Part II: Moment and Drag," *Proceedings of the AIAA Flow Control Conference*, June 2014.

[25] Lefebvre, A., and Zha, G.-C., "Numerical Simulation of Pitching Airfoil Performance Enhancement Using Co-Flow Jet Flow Control," AIAA Paper 2013-2517, 2013.

[26] Spalart, P., and Allmaras, S., "A One-Equation Turbulence Model for Aerodynamic Flows," AIAA Paper 1992-0439, 1992.

[27] Shen, Y.-Q., and Zha, G.-C., "Large Eddy Simulation Using a New Set of Sixth Order Schemes for Compressible Viscous Terms," *Journal of Computational Physics*, Vol. 229, No. 22, 2010, pp. 8296–8312.
doi:10.1016/j.jcp.2010.07.017

[28] Zha, G.-C., Shen, Y., and Wang, B., "An Improved Low Diffusion E-CUSP Upwind Scheme," *Computers and Fluids*, Vol. 48, No. 1, 2011, pp. 214–220.
doi:10.1016/j.compfluid.2011.03.012

[29] Shen, Y.-Q., and Zha, G.-Z., "Generalized Finite Compact Difference Scheme for Shock/Complex Flowfield Interaction," *Journal of Computational Physics*, Vol. 230, No. 12, 2011,
doi:10.1016/j.jcp.2011.01.039.

[30] Shen, Y.-Q., Zha, G.-C., and Wang, B.-Y., "Improvement of Stability and Accuracy of Implicit WENO Scheme," *AIAA Journal*, Vol. 47, No. 2, 2009, pp. 331–344.

[31] Shen, Y.-Q., Zha, G.-C., and Chen, X.-Y., "High Order Conservative Differencing for Viscous Terms and the Application to Vortex-Induced Vibration Flows," *Journal of Computational Physics*, Vol. 228, No. 2, 2009, pp. 8283–8300.
doi:10.1016/j.jcp.2009.08.004

[32] Shen, Y.-Q., and Zha, G.-C., "Improvement of the WENO Scheme Smoothness Estimator," *International Journal for Numerical Methods in Fluids*, Vol. 64, No. 6, 2010, pp. 653–675.
doi:10.1002/fld.2168

[33] Zha, G.-C., and Bilgen, E., "Numerical Study of Three-Dimensional Transonic Flows Using Unfactored Upwind-Relaxation Sweeping Algorithm," *Journal of Computational Physics*, Vol. 125, No. 2, 1996, pp. 425–433.

[34] Wang, B.-Y., and Zha, G.-C., "A General Sub-Domain Boundary Mapping Procedure for Structured Grid CFD Parallel Computation," *AIAA Journal of Aerospace Computing, Information, and Communication*, Vol. 5, No. 11, 2008, pp. 2084–2091.

[35] Lefebvre, A., Dano, B., Fronzo, M. D., Bartow, W. B., and Zha, G.-C., "Performance of a Co-Flow Jet Airfoil with Variation of Mach Number," AIAA Paper 2013-490, 2013.

[36] Wang, B. Y., and Zha, G.-C., "Detached-Eddy Simulation of a Co-Flow Jet Airfoil at High Angle of Attack," *AIAA Journal of Aircraft*, Vol. 48, No. 5, 2011, pp. 1495–1502.

[37] Im, H.-S., Zha, G.-C., and Dano, B. P. E., "Large Eddy Simulation of Co-Flow Jet Airfoil at High Angle of Attack," *Journal of Fluid Engineering*, Vol. 136, No. 2, 2014, p. 021101.

[38] Shen, Y.-Q., Zha, G.-C., and Wang, B.-Y., "Improvement of Stability and Accuracy of Implicit WENO Scheme," *AIAA Journal*, Vol. 47, No. 2, 2009, pp. 331–344.

[39] Wang, B. Y., and Zha, G.-C., "Detached-Eddy Simulation of Transonic Limit Cycle Oscillations Using High Order Schemes," *AIAA Journal of Aircraft*, Vol. 48, No. 5, 2011.